This project has received funding from the European Union's Horizon 2020 research and innovation programme under under FET-Open grant agreement no. 899646 (k-NET)

DELIVERABLE

Project acronym	k-NET
Project full title	k-Space Neural Computation with magnetic excitations
Grant Agreement no.	899646

Document title	Deliverable 1.2 – Report on spin-wave mode spectroscopy in the linear and nonlinear regimes
Revision no.	Final
Document date	27/02/2023
Dissemination level	Confidential
Responsible partner	CEA
Contributing partners	CEA, WWU, CREATE, CNRS, CSIC
Reviewing partners	All

CHANGE RECORD

Revision	Date	Changes	Authors	Status
1	23/02/2023	Version 1	G. de Loubens H. Merbouche	Not Submit-ted
2	24/02/2023	Version 2	A. Anane	
3	27/02/2023	Final version	G. de Loubens	Submit-ted

TABLE OF CONTENTS

1 MOTIVATIONS

k-NET will pursue the objective of engineering spin-waves (SW) eigenmodes representing small collective oscillations of the magnetization around the equilibrium configuration of a ferromagnetic medium. In confined geometries, SW modes are quantized (*i.e.*, only certain wavevectors are allowed in k-space), resulting in a discrete frequency spectrum. In the linear regime, SW modes can be considered as independent oscillators. However, the various interactions in ferromagnets can be described by an appropriate effective field, which itself depends on the magnetization, making SW dynamics, for sufficiently large deviations from the ground state, highly nonlinear. These intrinsic nonlinearities naturally couple the SW oscillations together. The objective of k-NET is to provide a proof of concept where this ensemble of discrete excitation modes (neurons) and their mutual couplings (synapses) are used as hardware for k-space based neural computing (k-NC). The control of the synaptic weights in this hardware can be achieved because nonlinear interactions between SW modes are predominantly determined by their amplitudes. Namely, the state of the system of SW modes, which can be controlled by external signals, defines how the energy (information) is channeled between different modes (neurons) by the nonlinearities (synapses). This enables programming the neural network defined in the k-space (k-NN).

Achieving this objective requires the design, fabrication and optimization of the k-NN devices and the characterization of their SW modes. All these tasks are part of WP1. This deliverable D1.2 reports on the efforts produced by the k-NET consortium to perform their SW mode spectroscopy in the linear and nonlinear regimes. This is mostly achieved using two complementary highly sensitive techniques that can map the SW modes in the direct and reciprocal spaces: micro-focused Brillouin light spectroscopy (μ-BLS) and magnetic resonance force microscopy (MRFM). These two methods have been employed to study the first and second generations of k-NET samples produced respectively in 2021 and 2022 based on the same high quality YIG film.

2 SPIN-WAVE MODE SPECTROSCOPY OF THE FIRST GENERATION OF SAMPLES

In this section, we present the spin-wave spectroscopy performed by means of MRFM and micro-focused BLS on the first generation of k-NN hardware, which was produced in 2021 based on a thin film of YIG of thickness about 60 nm (see deliverable D1.1). The k-NN hardware consists of YIG disks of diameter 0.5 µm, 1 µm, 3 µm and 5 µm, to which rf antennas were integrated to supply the microwave fields necessary to excite the SW modes. Spectroscopic characterization was performed both in the out-of-plane and in-plane configurations. The out-of-plane configuration conserves the cylindrical symmetry of the disks, which simplifies the identification of the SW modes; it is also well-suited to extract the damping parameter, thanks to the large splitting between modes, that is favorable to extract the linewidth of the resonance peaks. The in-plane configuration is particularly relevant to the k-NET project, as it favors nonlinear interactions between SW modes, due to the ellipticity of magnetization trajectory. It is therefore of crucial importance to perform linear and nonlinear SW mode spectroscopy in this configuration. **Figure 1** gives an overview of these two configurations and of the sample geometry.

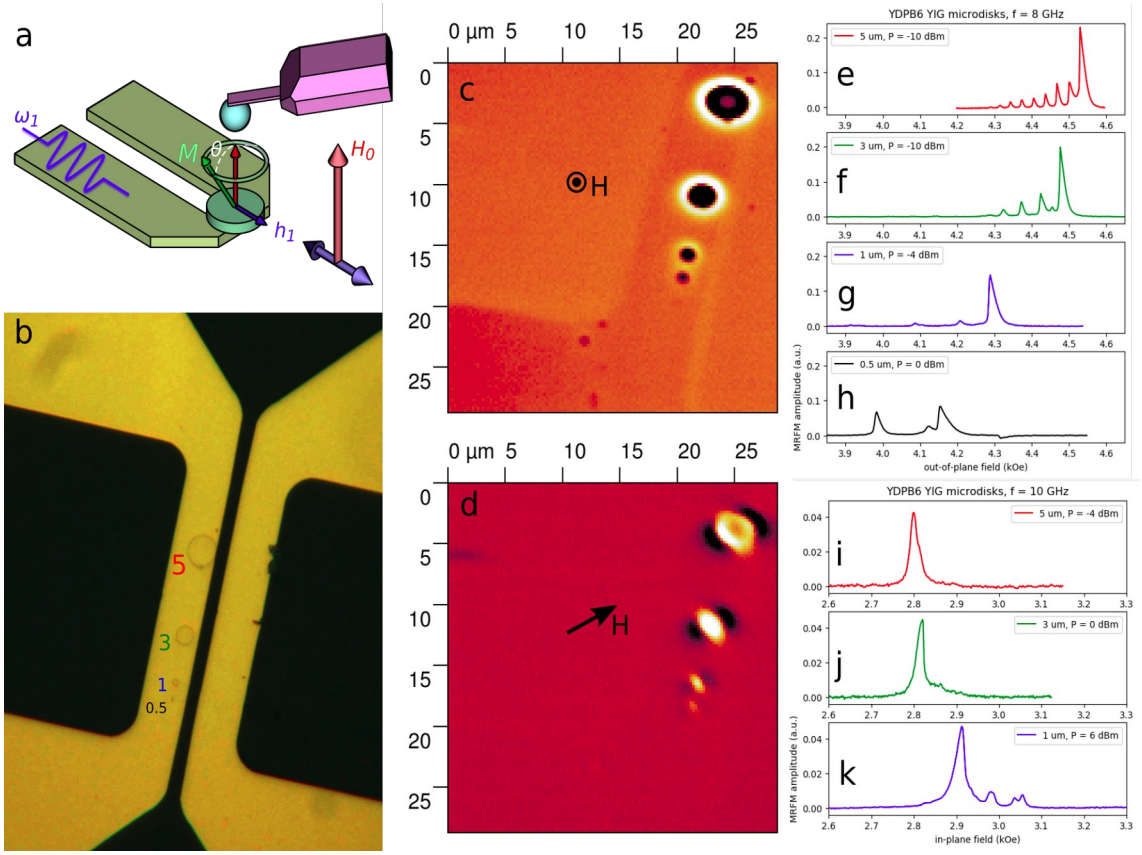

Figure 1. *MRFM spectroscopy of the first generation of k-NET hardware. (a) MRFM schematics. (b) Optical image of the sample. (c) MFM imaging with an out-of-plane field H = 4 kOe. (d) MFM imaging with an in-plane field H = 4 kOe. (e-h) Out-of-plane MRFM spectroscopy at 8 GHz of the 5, 3, 1 and 0.5 µm diameter disks. (i-k) In-plane MRFM spectroscopy at 10 GHz of the 5, 3, and 1 diameter disks.*

2.1 Linear SW MRFM spectroscopy in the out-of-plane configuration

2.1.1 SPIN-WAVE SPECTROSCOPY VS. DISK DIAMETER: RADIAL SW MODES

Figures 1e-h display the out-of-plane MRFM spectroscopy of the 5 µm, 3 µm, 1 µm and 0.5 µm disks, respectively, at 8 GHz. Typical standing SW mode spectra are observed. As the disk diameter decreases,

the main resonance peak shifts to lower field, and the splitting between higher order SW modes increases, which is due to the stronger geometric confinement. Note that the spectrum of the 0.5 µm diameter disk clearly deviates from the other three disks, as it displays two peaks of almost similar amplitude, instead of a series of weaker harmonics as the field is decreased. We attribute this to some degradation induced by the nanofabrication.

Due to selection rules and to the spatial homogeneity of the in-plane excitation field produced by the antenna on top of the disks, it is expected that only radial SW modes (with azimuthal mode number equal to zero) are excited in the experiment. To analyze the linear SW spectroscopy of the YIG disks in out-of-plane configuration, we performed micromagnetic simulations. The magnetization and gyromagnetic ration used in the simulation are extracted experimentally from broadband MRFM measurements (see section 2.1.2). The damping is set to 10^{-3}. The diameter is the nominal diameter, and the thickness, which is only known approximately due to the LPE growth of the thin film, is varied. **Figure 2** presents the comparison for the out-of-plane geometry between the experimental SW spectra of the different disks (bottom row) and the simulated SW spectra using micromagnetic simulations (top and middle rows corresponding to different thicknesses, t=66 nm and t=52 nm, respectively). As expected, the simulated SW modes correspond to radial eigenmodes, as seen from the insets displayed in the upper left panel. It clearly appears that for the 5 µm (left column) and 3 µm disks (middle column), the simulated SW spectra almost perfectly match the experimental ones using a YIG thickness of 52 nm. However, such a good agreement is not observed for the 1 µm diameter disk, which we attribute to the relative importance of the disk periphery, that is damaged during the nanofabrication process, with respect to the total volume of the disk. Most likely, this experimental SW spectrum would be more accurately reproduced using a spatial gradient of magnetic properties at the disk boundaries.

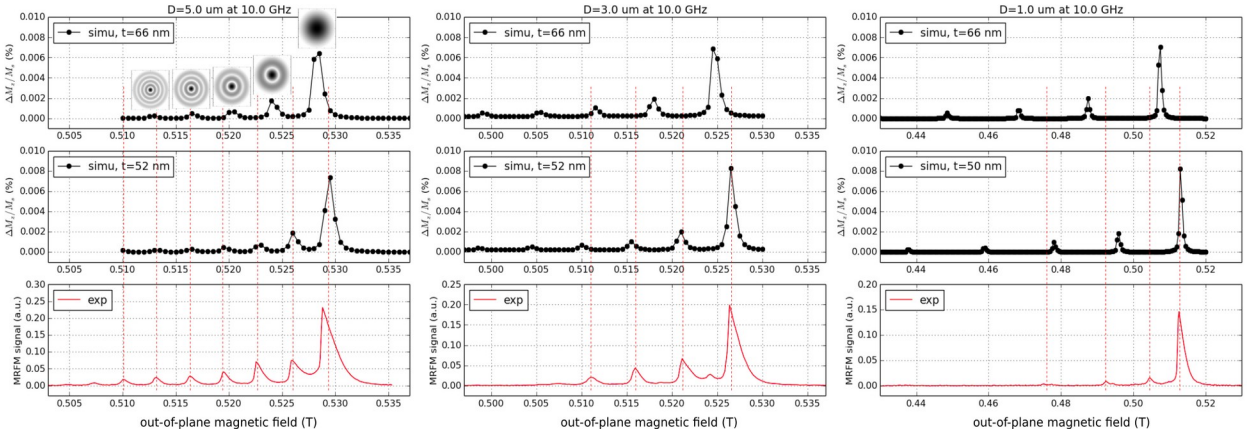

Figure 2. *Comparison of experimental out-of-plane SW mode spectroscopy (bottom row) to micromagnetic simulations using a YIG thickness of 66 nm (top row) and 52 nm (middle row). Each column corresponds to a different disk diameter: 5 µm (left), 3 µm (middle) and 1 µm (right). Insets in the upper left panel display the spatial profiles of the radial SW modes.*

2.1.2 BROADBAND SW MODE SPECTROSCOPY: INCREASED DAMPING VS. REDUCED DIAMETER

Due to the large mode splitting, the out-of-plane configuration is well-suited to extract the damping parameter. For this, broadband FMR spectroscopy is performed at low microwave power, to remain in the linear regime. For each frequency from 2 GHz to 20 GHz by step of 0.5 GHz, the MRFM spectrum is recorded as a function of field. An example of such broadband SW spectroscopy is presented for the 3 µm diameter disk in **Figure 3**.

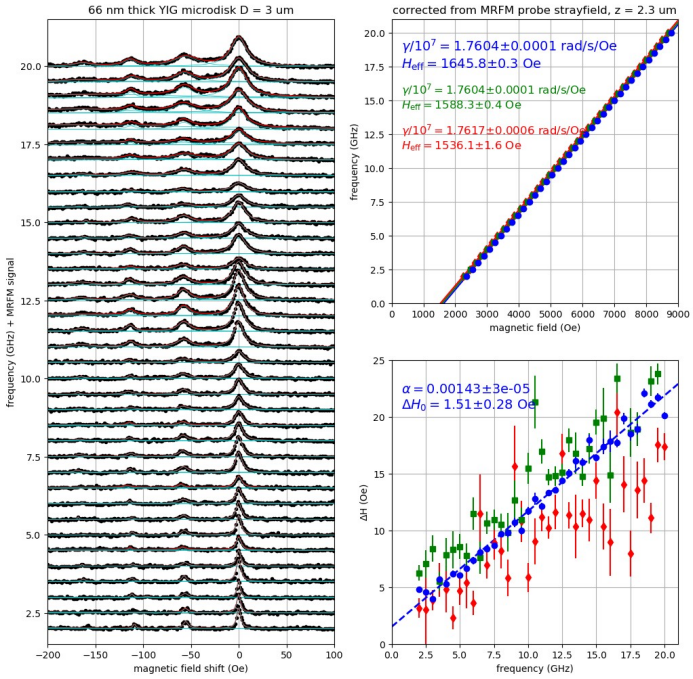

Figure 3. *Broadband out-of-plane MRFM spectroscopy of the 3 µm diameter disk in the perpendicularly saturated state. The left panel shows the individual spin-wave spectra and their multi-peak Lorentzian fits as a function of frequency in the range 2 – 20 GHz. The top right panels shows the frequency-field evolution of the three main peaks and their linear fits using the Kittel formula. The bottom right panel shows the dependence of their linewidths on frequency. The linear fit of the main peak's linewidth yields the Gilbert damping parameter.*

By fitting the SW spectra with the appropriate number of Lorentzian lines, one can extract the resonance fields and linewidths of the different peaks as a function of frequency. Fitting the dispersion relation with the standard Kittel formula:

$$\omega = \gamma\left(H - H_{eff}\right)$$

one can extract the gyromagnetic ratio γ and the effective field H_{eff} corresponding to each of the fitted SW modes (top right panels). As expected, the former is equal to 1.76 10^7 rad/s/Oe, very close to the value obtained in the thin film, for all the disks. The effective field of the main FMR peak decreases with the disk diameter, due to the finite size effects on the demagnetization field in the disk. Fitting the linear evolution of the main peak's linewidth upon frequency with the formula:

$$\Delta H = \Delta H_0 + \frac{2\alpha\omega}{\gamma}$$

one can extract the Gilbert damping parameter α and the inhomogeneous contribution ΔH_0 to the linewidth (bottom right panels). While the latter is negligible in the out-of-plane geometry for the different disks (2 Oe at most), the extracted damping parameters are much larger in the patterned YIG disks (in the low 10^{-3} range), than in the extended YIG film (below 10^{-4}). We note that although the fitted linewidths of higher order modes have larger error bars than those of the main mode (compare green/red dots with blue dots in lower right panel of **Figure 3**), the same value of damping can be used to fit their frequency dependence.

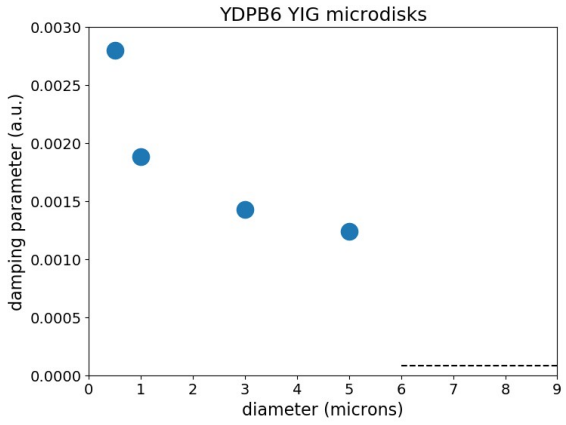

Figure 4. *Evolution of the damping parameter extracted from broadband MRFM spectroscopy as a function of disk diameter. The dashed line shows the damping measured in the thin film.*

To elucidate the origin of this increased damping parameter, its dependence on disk diameter is plotted in **Figure 4**, together with the value extracted on the extended thin film, shown as the horizontal dashed line. The damping parameter continuously increases from 0.0012 to 0.0028 with the disk diameter decreasing from 5 µm down to 0.5 µm, *i.e.*, 20 to 40 times the initial damping of the thin film. The inverse power law, which seems to govern the observed tendency, points towards a degradation of magnetic properties at the circumference of the disks.

2.2 Linear SW spectroscopy in the in-plane configuration

2.2.1 MRFM SPECTROSCOPY: DEPENDENCE OF SPIN-WAVE SPECTRUM ON DIAMETER

Figures 1h-j display the in-plane MRFM spectroscopy of the 5 µm, 3 µm and 1 µm disks, respectively, at 10 GHz. The observed SW mode spectra are composed of a main central line, with low and high field tails, and several other modes having much lower amplitude can be detected at both lower and higher applied field. The identification of SW modes is therefore more complex than in the out-of-plane geometry. For this we again used micromagnetic simulations, as shown in **Figure 5**. The agreement between simulated and measured SW spectra for the 5 µm and 3 µm disks is reasonable. In both cases, it is difficult to spectroscopically resolve the different modes for a damping parameter in the 10^{-3} range. The case of the 1 µm diameter disk is shown in the right most panels. As in the out-of-plane configuration, none of the two different values of thickness used in the simulations allows to accurately reproduce the experimental data. In particular, the simulated SW modes localized at the edges along the field direction observed at higher field are not observed experimentally, despite their sizable amplitude. We attribute this experimental fact to the problem of edge deterioration by the nanofabrication process, already raised above. Most likely, the periphery region has degraded magnetic parameters and a substantially higher damping than the central region of the disk, preventing the experimental observation of these SW edge modes. The situation around the most intense mode is more favorable, since we observe that the hierarchy in the relative peak amplitudes, and, to a less extent, the peak splittings, are almost reproduced by simulations.

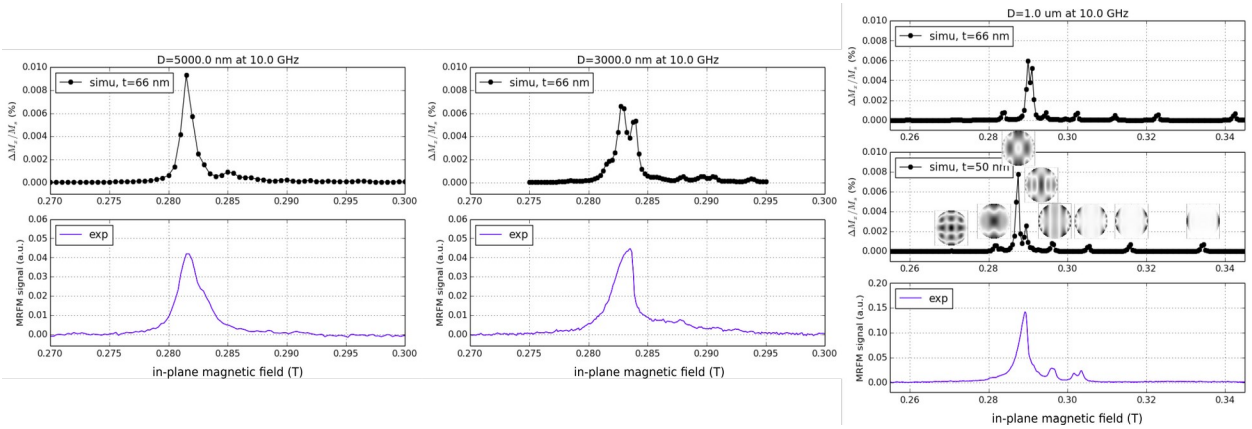

Figure 5. *Comparison of experimental in-plane SW mode spectroscopy (bottom row) to micromagnetic simulations using a YIG thickness of 66 nm or 50 nm, as indicated in the legend. Each column corresponds to a different disk diameter: 5 µm (left), 3 µm (middle) and 1 µm (right). Insets in the right middle panel display the spatial profiles of the modes excited by the uniform microwave excitation.*

2.2.2 BLS SPECTROSCOPY OF THE 1 MICRON YIG DISK

Micro-focused BLS was also used to perform SW mode spectroscopy in the linear regime. A sketch of the experimental configuration is shown in **Figure 6a**. The reported data have been obtained on a 1 µm diameter YIG disk, positioned underneath the signal line of a GSG micro-antenna, as shown in **Figure 6b**. To measure the low power transverse FMR spectrum of this disk, shown in **Figure 6c**, the in-plane ap-

plied field is fixed to $\mu_0 H_0$ = 50 mT and the intensity of the inelastically scattered light is plotted *vs.* the frequency of the microwave current supplied into the rf antenna. One observes an FMR line centered at 2.86 GHz, with sizable low and high frequency tails. At the maximum, the dynamical magnetization is localized in a large central zone of the disk, as demonstrated by rastering the laser beam on the disk area and recording the BLS amplitude to image the mode profile shown in the inset. Similar imaging mode is used to reveal the spatial profile of the magnetization dynamics excited as a function of microwave frequency, as for instance at 3 GHz, where the mode profile displays two symmetric maxima in the transverse direction to the applied field. Besides this main FMR line around 2.86 GHz, the BLS spectrum also shows a peak at much higher frequency, typically between 9 and 12 GHz as the applied field is varied between 60 and 140 mT (see **Figure 6d**). This peak is associated to the first thickness mode, or perpendicular standing spin-wave (PSSW), with a sinusoidal profile of the dynamic magnetization along the film thickness. Using the standard value of exchange constant of YIG, one can plot the PSSW frequency as a function of field, shown by the dashed lines in **Figure 6e**, for three different values of the YIG thickness. From these measurements, it is deduced that the YIG film is thinner, 52 nm, than expected from preliminary X-ray data (66 nm).

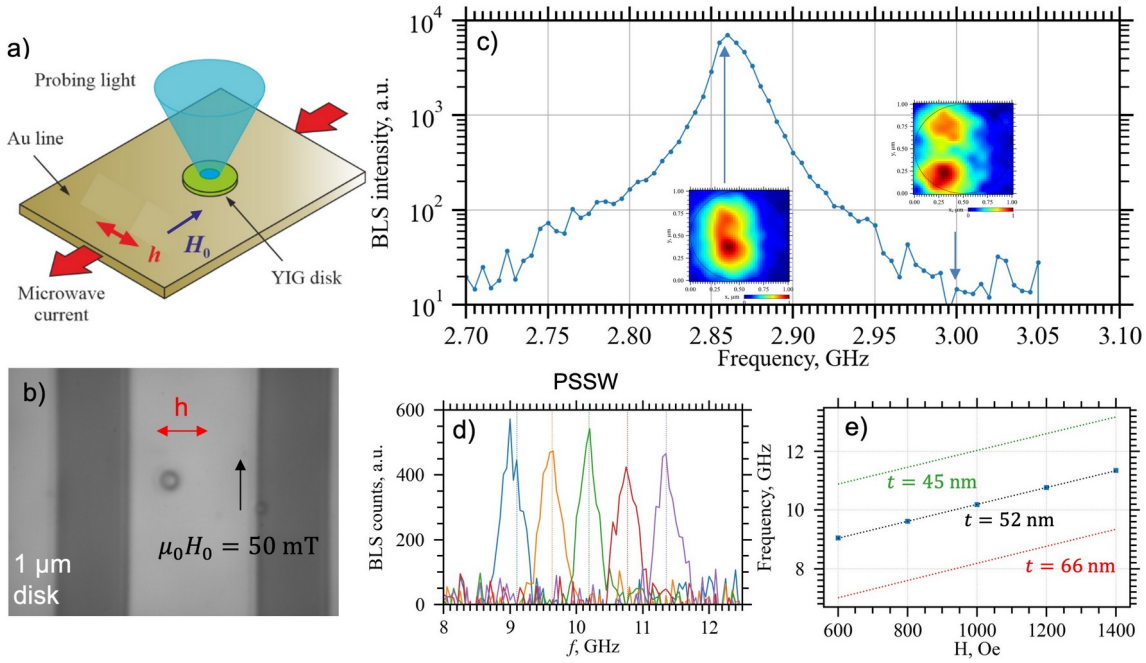

Figure 6. *μ-BLS characterization of the 1 μm diameter YIG disk. (a) Schematics of the μ-BLS experiment. (b) Optical image of the measured sample. (c) BLS spectrum at $\mu_0 H_0$ = 50 mT applied in the plane. Insets are the μ-BLS maps of the spatial profiles of dynamic magnetization excited at two different frequencies. (d) Detection of the first thickness mode and (e) its dependence on the applied field, together with analytical predictions for three different values of the YIG film thickness.*

2.3 Nonlinear SW spectroscopy in the in-plane configuration

The most standard way to excite SW modes in a magnetic microstructure is by direct inductive coupling, where the quasi uniform microwave field produced on the magnetic volume by an rf antenna couples to the transverse dynamical component of magnetization associated with the SW modes, with a maximal efficiency when the applied rf frequency coincides with the eigenfrequency of the mode. However, this method is not adapted to excite modes with anti-symmetric spatial profiles (their overlap integral with the excitation field is zero), nor short-wavelength modes (their excitation efficiency quickly decreases with their wavevector). Yet, these two categories of modes make up a significant part of the k-space. In order to excite a large number of modes, the method of parametric (or parallel) pumping, which does not suffer from these limitations, was therefore employed (as in Task 2.1 of WP2). In this case, the mi-

crowave magnetic field created by the rf antenna is aligned parallel to the static field. As a result, this field does not couple to the SW modes directly. Instead, it can be considered as a dynamic modulation of the static parameter of the system – the strength of the static bias field. Under these conditions, the excitation field is able to induce magnetization dynamics via the parametric resonance process, when its frequency becomes equal to twice the frequency of a SW mode, and its amplitude exceeds the parametric – nonlinear – threshold, which depends on the mode relaxation (the lower, the lower the threshold) and on the mode ellipticity (the larger, the lower the threshold).

2.3.1 MRFM PARAMETRIC SW MODE SPECTROSCOPY VS. DIAMETER

In the following measurements, the dc magnetic field is applied in-plane at an angle of 45° with respect to the direction of the rf magnetic field. Therefore the rf field excitation has both a transverse and a parallel component relative to the magnetization direction. The parallel pumped SW spectrum is studied for different-sized disks as a function of the applied microwave power. **Figure 7** shows the results of the MRFM parametric spectroscopy performed at a constant microwave frequency of 4 GHz for the 1, 3 and 5 µm diameter disks (color-coded intensity maps), together with the corresponding transverse excitation spectra measured at fixed frequency of 2 GHz and power of -5 dBm (continuous white curves). Only a few SW modes are detected in the latter regime, as it was the case in **Figures 1i-k** and **Figure 4**. In contrast, we observe that a large number of modes can be excited by parallel pumping at 4 GHz for all the disks, in the range of applied dc field corresponding to the direct excitation of modes at 2 GHz, because parametrically excited modes are generated at half the pumping frequency. As expected, this occurs only above a minimum power level, that ranges from about -4 dBm for the 5 µm disk to -2 dBm for the 1 µm disk. The fact that the parametric threshold increases and that the density of the excited modes decreases as the lateral size decreases can be explained by geometrical confinement effects.

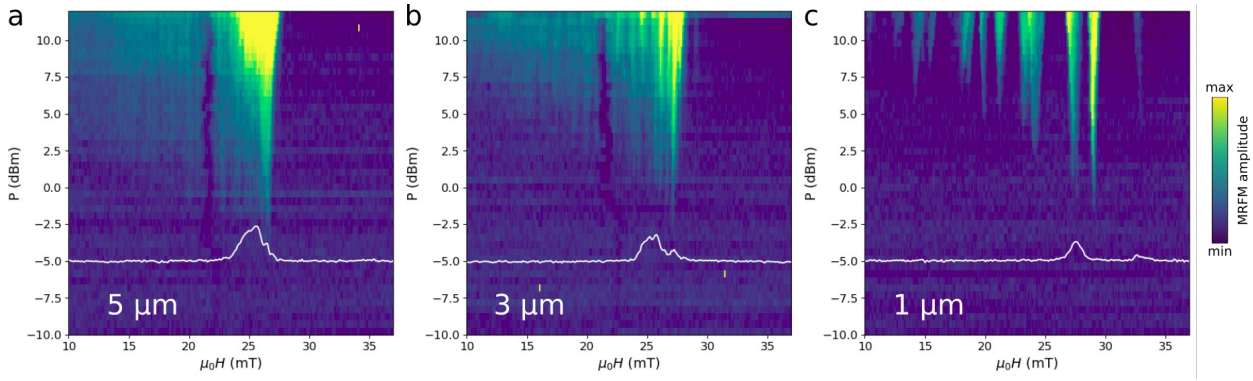

Figure 7. *Intensity maps of the parametric modes in the field-power coordinates excited by the microwave field of frequency 4 GHz, measured by MRFM on the 5 µm (a), 3 µm (b) and 1 µm (c) diameter YIG disks. In each panel, the continuous white curve corresponds to the direct excitation spectrum at the frequency of 2 GHz. The rf pumping field is at 45° from the dc field.*

2.3.2 IDENTIFICATION OF SPIN-WAVE EIGENMODES EXCITED BY PARAMETRIC PUMPING IN THE 3 MICRON YIG MICRODISK

In the following, we will mainly focus on the 3 µm disk where the SW modes are quite abundant but at the same time discernible (not too closely spaced). We perform similar measurements on this disk, this time fixing the value of the dc field to 27 mT, and scanning the parallel pumping frequency as a function of the microwave power. **Figure 8b** shows the intensity map of the parametrically excited modes in these conditions, as a function of half the pumping frequency $f_p/2$ and the rf power P, varied along the horizontal and vertical axes, respectively. The mode with the lowest power threshold $P_{th,min}$ = -3 dBm is excited at the pumping frequency of f_p = 3.95 GHz, *i.e.*, it has a frequency of $f_p/2$ = 1.975 GHz. As the power is increased beyond this minimal threshold, the number of modes which become parametrically

excited, also increases. For instance, at a power of 4 dBm, there are at least 20 different modes, whose frequencies span from $f_p/2$ = 1.95 GHz to $f_p/2$ = 2.3 GHz, which can be excited.

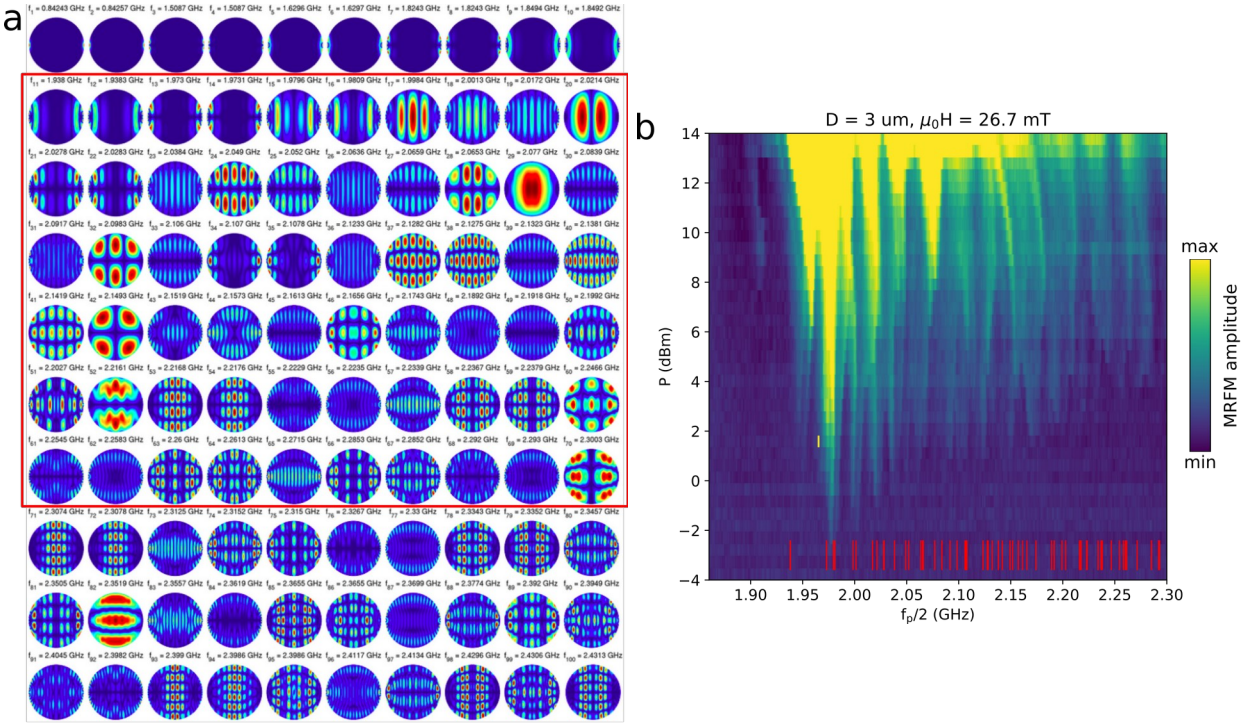

Figure 8. *(a) Computed spatial profiles of the 100 lowest frequency modes of the 3 µm diameter YIG disk, in-plane magnetized by a field of 27 mT. The color code refers to the oscillation amplitude of the local magnetization, from blue (minimum) to red (maximum). (b) Comparison between parametric spectroscopy MRFM data (color-coded intensity map) and computed eigenfrequencies (red vertical ticks) of modes 11 to 70 (surrounded by the red rectangle in panel (a)).*

Micromagnetic computation of spin-wave eigenmodes

In order to identify these parametrically excited modes, micromagnetic simulations using an eigenmode solver developed in the consortium have been performed to calculate the SW spectrum. Shortly, the magnetic ground state is first computed for the specific geometry and applied magnetic field. Once the magnetic ground state is known, the equation describing magnetization dynamics, the Landau-Lifshitz-Gilbert (LLG) equation, is linearized around the ground state and small oscillations mode spatial profiles are computed. This problem can be formulated as an eigenvalue problem as described in the paper [M. d'Aquino et al., *J. Comput. Phys.* **228** , 6130 (2009)]. The solution of the eigenvalue problem leads to the determination of the SW spectrum of the magnetic sample under investigation.

Here, the geometry of the body, a 50 nm thick disk of 3 µm in diameter, was discretized using 300x300x5 cubic cells (mesh size of 10x10x10 nm^3), and the values of the magnetic parameters used in the simulation were determined experimentally by broadband FMR spectroscopy in the linear regime: gyromagnetic ratio $\gamma/(2\pi)$ = 28.28 GHz/T, magnetization M_s = 140.7 kA/m. The exchange constant of YIG was taken from literature: A = 3.7 pJ/m [S. Klingler et al., *J. Phys. D: Appl. Phys.* **48**, 015001 (2015)]. As in the experimental case, the applied field lies in the plane of the disk, and is set to 27 mT.

Figure 8a displays the computed spatial profiles of the 100 first eigenmodes. The 10 lowest frequency modes (first row) correspond to edge modes, where the precession of magnetization is strongly confined at the boundaries of the disk, in the (horizontal) direction of the applied dc field. The following modes correspond to standing SW modes, which can be labeled by the number of precession lobes in the horizontal (n_x) and vertical (n_y) direction. For instance, mode 20 (second row, last column) can be la-

beled by n_x=2 and n_y=1, i.e., it is the (2,1) mode. Mode 40 (fourth row, last column) is the (11,3) mode. The most uniform mode, usually referred as the FMR mode, is mode 29, or mode (1,1).

Figure 8b presents the comparison between the experimental spectroscopy and the computed eigenfrequencies of modes 11 to 70, shown as red ticks on top of the intensity map of the parametrically excited modes. We observe a good agreement between the computed mode frequencies and the experimental mode frequencies (or half-pumping frequencies $f_p/2$) observed at the bottom of the parametric instability regions (elongated yellow-green triangles / fingers pointing downwards on the intensity map). From this comparison, it is possible to state that *almost all*, if not *all* SW eigenmodes, can be parametrically excited, whatever their spatial profile. Due to the high density of modes in the investigated frequency range, we will only focus on a few modes, to emphasize the good agreement noted above. The lowest lying computed modes on **Figure 8b** are the pair of modes 11 and 12 with respective frequencies 1.938 and 1.9383 GHz, which correspond rather well to the measured parametric instability region with a threshold power of 2 dBm at around 1.95 GHz. The small disagreement of 10 MHz between the computed and measured frequencies is not unexpected, since these modes belong to the categories of edge modes, and we have previously shown that the nanofabrication process modifies the magnetic properties at the boundaries of the YIG disks, which is not taken into account in the simulations. If we move to the next parametrically excited modes, which have the lowest power threshold and have frequencies around 1.975 GHz, the comparison with computed frequencies shows that they correspond to two pairs of modes: modes 13 and 14 with respective frequencies 1.973 and 1.9731 GHz, and modes 15 and 16, at 1.9796 and 1.9809 GHz. The next excited modes in the experimental spectroscopy map are at around 2 GHz, and they correspond to modes 17 at 1.998 GHz and mode 18 at 2.001 GHz. As a matter of fact, a detailed inspection of the data shows that indeed, the parametric instability region has two nearby minima with frequencies equally spaced around 2 GHz. This good agreement between experimental and computed mode frequencies continues over the full range of investigated frequencies. We note that among the 60 modes whose frequencies have been plotted in **Figure 8b**, only 44 modes have discernible frequencies and spatial profiles, a few of them being pairs of modes with very similar characteristics (e.g., pairs of modes 11 and 12, 13 and 14, 15 and 16, 21 and 22, etc.).

Experimental spatial profiles of parametric modes

To push further the comparison between computed SW modes and experiments, it is possible to take advantage of micro-focused BLS, which offers the possibility of mapping out the spatial profiles of dynamic magnetization in microstructures. This BLS imaging has been performed on a similar 3 µm YIG disk as the one measured by MRFM in **Figure 8b**, under an in-plane bias field of 30 mT. To compare the experimental mode profiles with the computed mode profiles, the micromagnetic simulations have therefore been repeated at 30 mT as well. To avoid nonlinear distortions of the mode profiles, known to occur when the mode amplitude increases too much, the BLS mapping of the mode profiles was performed at small super-criticality, *i.e.*, at the bottom of the mode instability region. A dozen of different modes were imaged, **Figure 9** presents the comparison between the experimental and computed profiles of ten of them. Overall, the measured profiles are in good agreement with the computed ones, taking into account the experimental spatial resolution (~ 250 nm) and the long duration of these measurements, which are subjected to experimental drifts. Similarly to the analysis performed in **Figure 8b**, we also observe a good agreement between the experimental and computed mode frequencies, with a mismatch that remains under 13 MHz for all modes.

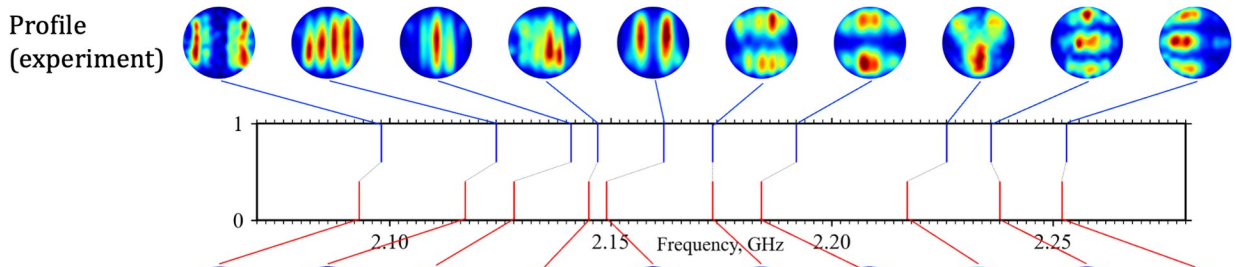

f_{exp} (GHz)	2.098	2.124	2.141	2.147	2.162	2.173	2.192	2.226	2.236	2.253
f_{simu}(GHz)	2.093	2.117	2.128	2.145	2.149	2.173	2.184	2.217	2.238	2.252
$f_{exp} - f_{simu}$ (MHz)	5	7	13	2	13	0	8	9	−2	1

Figure 9. *BLS imaging of mode profiles. The central graph displays the BLS detected frequencies at 30 mT for 10 modes of the 3 µm disk (blue lines) and the corresponding computed frequencies of eigenmodes (red line). These frequencies are matched (dotted dark lines) by associating the mode profiles measured in the experiment (above the graph) to the ones computed in the simulation (below). The experimental and simulated mode frequencies (in GHz) and their difference (in MHz) are given in the table.*

2.3.3 BLS PARAMETRIC SW SPECTROSCOPY OF THE 1 MICRON YIG MICRODISK

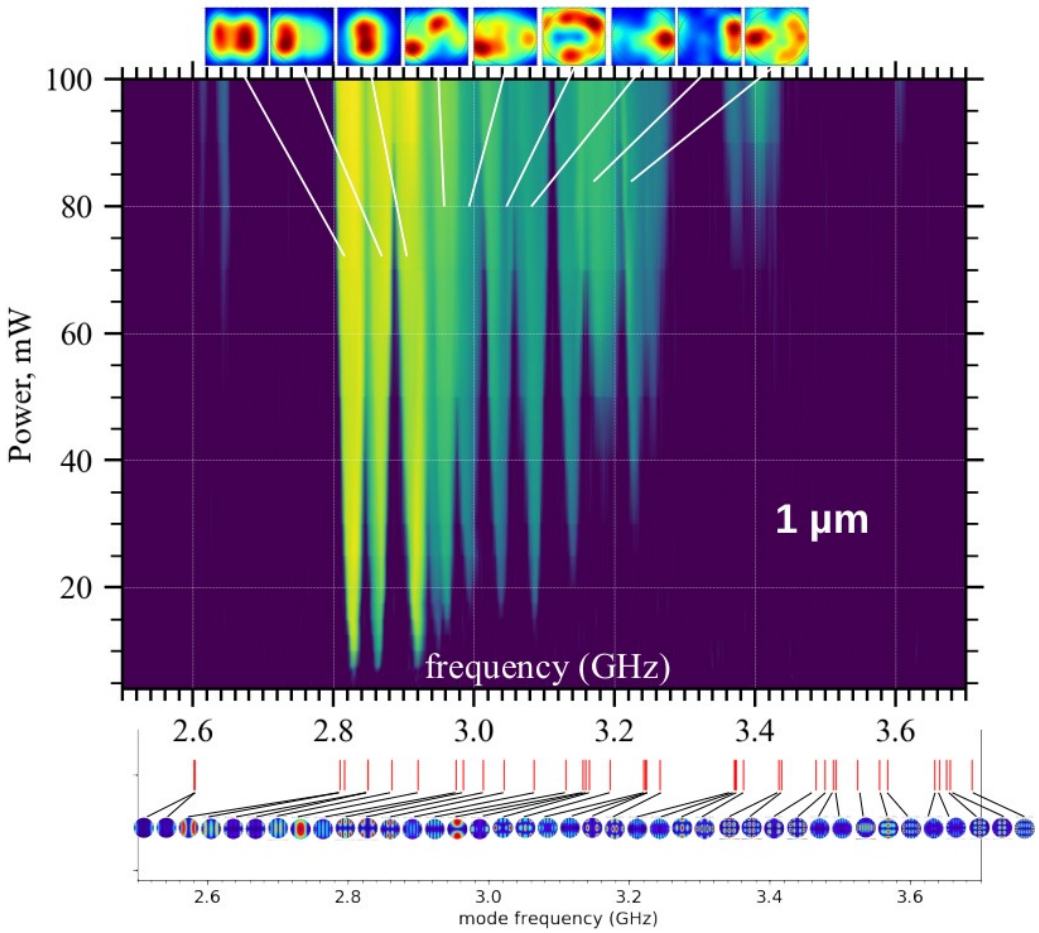

Figure 10. *BLS parametric spectroscopy of the 1 µm YIG disk performed under an in-plane bias field of 50 mT. The insets at the top of the figure present some of the experimental mode profiles. The bottom of the figure shows the computed mode frequencies and corresponding profiles.*

A similar study has also been performed on the 1 µm YIG disk, and is presented in **Figure 10**. It is observed that the global distribution of modes is well reproduced by simulations, however, the measured mode profiles are more complex than simulated. We ascribe these discrepancies to the previously mentioned degradation of disk periphery during the nanofabrication process.

2.4 Conclusion on the first generation of k-NET hardware

Thanks to the comparison between parametric spectroscopy and mode imaging respectively performed by MRFM and BLS on one side, and micromagnetic simulations on the other side, we have successfully excited, detected and identified a large number (> 40) of SW eigenmodes in the 3 µm YIG disk, where the mode density is large due to the large lateral dimensions. The computed spatial profiles provide a direct way to label those modes, using the numbers of precession nodes in the directions parallel (n_x) and transverse (n_y) to the applied magnetic field. These results therefore validate the milestone M1.1 "Successful spectroscopic labeling of a large number of modes (>10)". A detailed report on this nonlinear parametric SW spectroscopy can be found in the following paper submitted to Phys. Rev. Appl. and posted on arXiv (https://doi.org/10.48550/arXiv.2301.13468): *Complete identification of spin-wave eigenmodes excited by parametric pumping in YIG microdisks* by T. Srivastava, H. Merbouche, et al.

The SW mode spectroscopy presented above allowed us to precisely extract the thickness of the YIG layer, found to be 52 nm. However, the SW mode spectroscopy performed on this first generation of samples also provided indications, that some damages are induced during the nanofabrication process at the disk boundaries. They result in a severely increased damping as the diameter of the disk is reduced, which is detrimental to the reach nonlinear thresholds, such as the parametric threshold, at reasonably low power injected in the integrated rf antennas. Moreover, they also lead to complications in the identification of modes of the smaller disks (diameter of 1 µm and below), which can eventually jeopardize the training process for neuromorphic computation. In particular, edge modes, which constitute the dominant modes in the low frequency part of the excitation spectrum, are strongly affected by these modifications of the disk periphery. For the increased damping, we note that in this first generation of samples, there was a direct contact between the Ti underlayer of the antenna, and the YIG material at the periphery of the disks. This could lead to some undesired oxidation of YIG, and might also add some additional relaxation channel for SW dynamics due to spin pumping in the adjacent metallic rf antennas.

Based on these findings, the nanofabrication process has been improved for the second generation of k-NN hardware, as detailed in section 3.

3 SPIN-WAVE MODE SPECTROSCOPY OF THE SECOND GENERATION OF SAMPLES

The design of the second generation of k-NET hardware has been adapted based on the results of the previous SW mode spectroscopy performed on the first generation. It is presented in **Figure 11**. The major changes made to the sample design are the following:

- Insertion of a 50 nm thick insulating layer above the disks to prevent any contact with the rf antennas' underlayer of Ti.
- Narrower width of rf antennas (8 µm → 3 or 4 µm) to provide larger excitation fields at similar input powers and reach relevant nonlinear regimes more easily.
- Larger variation in sample geometry (lateral dimensions, circular vs. elliptical shapes) to study in more details the impact of finite size effects on SW mode spectrum.
- Devices located under and next to rf antennas to evaluate potential impact on damping.

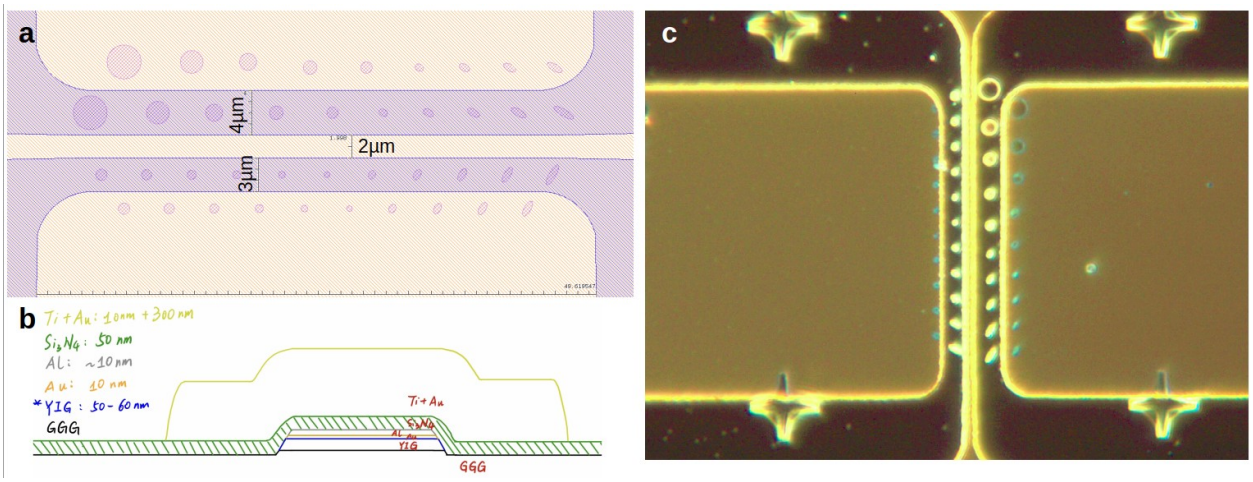

***Figure 11**. (a) Design of second generation of samples used for MRFM SW mode spectroscopy. (b) Cross-section of the sample showing in dashed green the insulating Si_3N_4 layer introduced between the YIG microdisks and the Ti+Au antenna. (c) Optical image of the actual sample introduced in the MRFM set-up.*

3.1 MRFM linear SW mode spectroscopy

3.1.1 DEPENDENCE OF SPIN-WAVE SPECTRUM ON DIAMETER

Out-of-plane configuration

Using MRFM, SW mode spectroscopy as a function of disk diameter has been conducted in the out-of-plane geometry, as summarized in **Figure 12**. As for the first generation of samples, one clearly observes the impact of confinement on the radial SW mode spectrum. As the disk diameter decreases, the main resonance peak shifts to lower field, and the splitting between higher order SW modes increases.

An unexpected result, which can be straightforwardly observed on the raw spectra of **Figure 12**, is that the linewidths of the resonance peaks decrease with the disk diameter, which is exactly the opposite as what was observed on the previous generation of samples (cf. **Figure 4**). We will comment on this result further below.

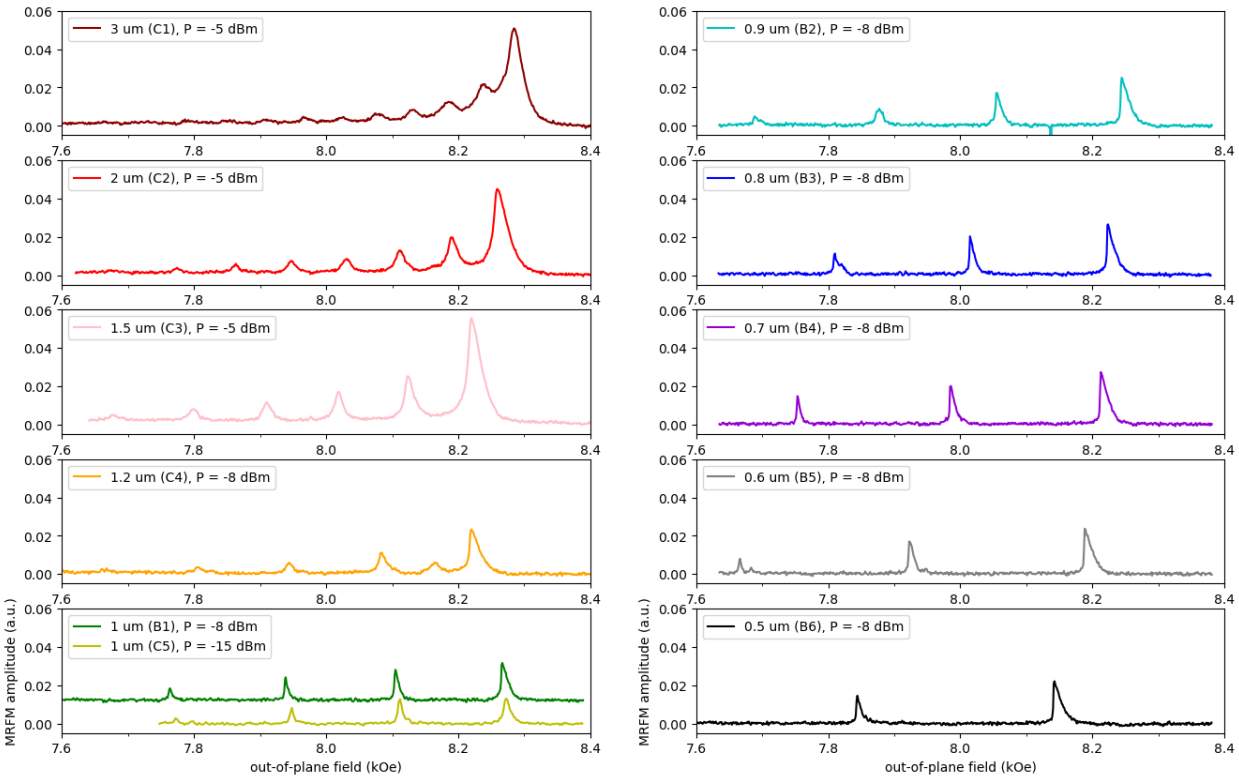

Figure 12. *Out-of-plane SW spectroscopy at 19 GHz of the different disks located under the rf antennas.*

In-plane configuration

Similar SW mode spectroscopy has been performed with the disks magnetized in the plane, as displayed in **Figure 13**. In these experiments, the MRFM probe is a little bit far from the disks, therefore a pretty large excitation power had to be used, which explains the nonlinear shape of the main mode observed.

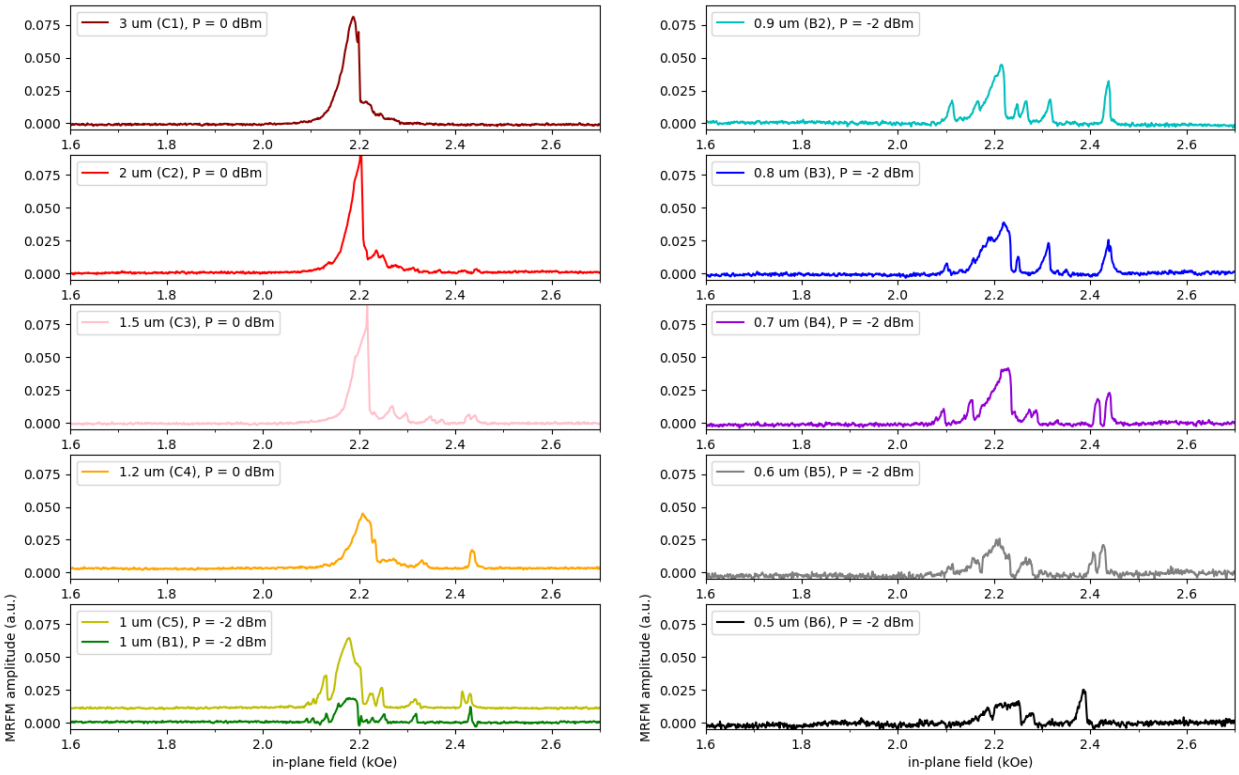

Figure 13. *In-plane SW spectroscopy at 8 GHz of the different disks located under the rf antennas.*

After approaching the MRFM probe closer to the smaller disks (diameter below 1 µm) located next to (disks "A") or under (disks "B") the 3 µm wide rf antenna, a mode precise in-plane SW mode spectroscopy has been performed at 8 GHz. It is shown in **Figure 14**. For each disks in the A and B series, we observe intense bulk modes located at about 2.2 kOe, and several modes at higher fields (> 2.3 kOe), which are ascribed to edge modes. The simple fact, that we easily observe the latter, points towards a greatly improved quality of disk periphery, with respect to the previous generation of samples.

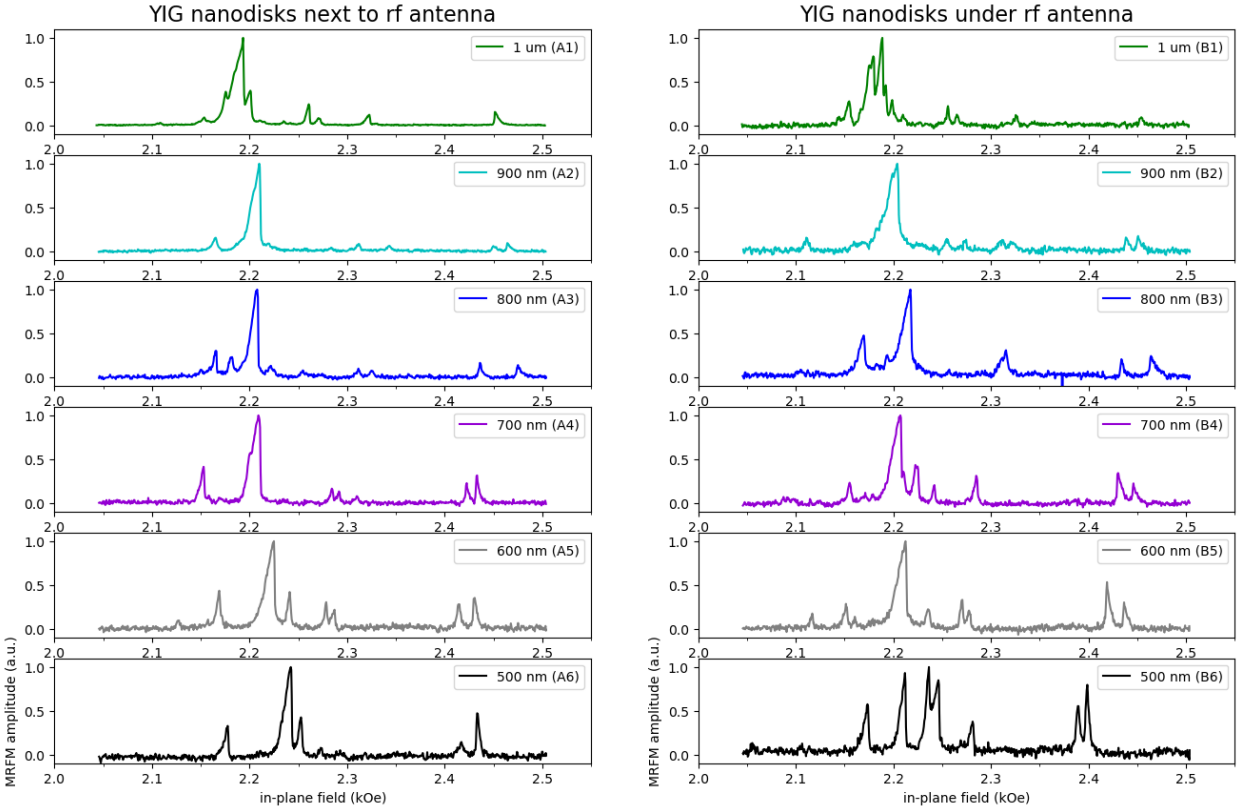

Figure 14. *Comparison of in-plane MRFM SW spectroscopy at 8 GHz between the YIG nanodisks next to the rf antenna (left) and under the rf antenna (right).*

3.1.2 COMPARISON TO MICROMAGNETIC SIMULATIONS

In order to demonstrate the improved quality of the second generation of samples we compare the out-of-plane and in-plane SW spectra of the 1 µm disks of the first and second generation to micromagnetic simulations in **Figure 15**.

In both configurations, we observe an improved agreement between the simulated spectrum using a YIG thickness of 50 nm (second row) and the experimental spectrum. In the out-of-plane geometry, the splitting between radial modes is much better reproduced. In the in-plane geometry, we now detect experimentally several of the edge modes, whose position is reasonably well reproduced by simulations.

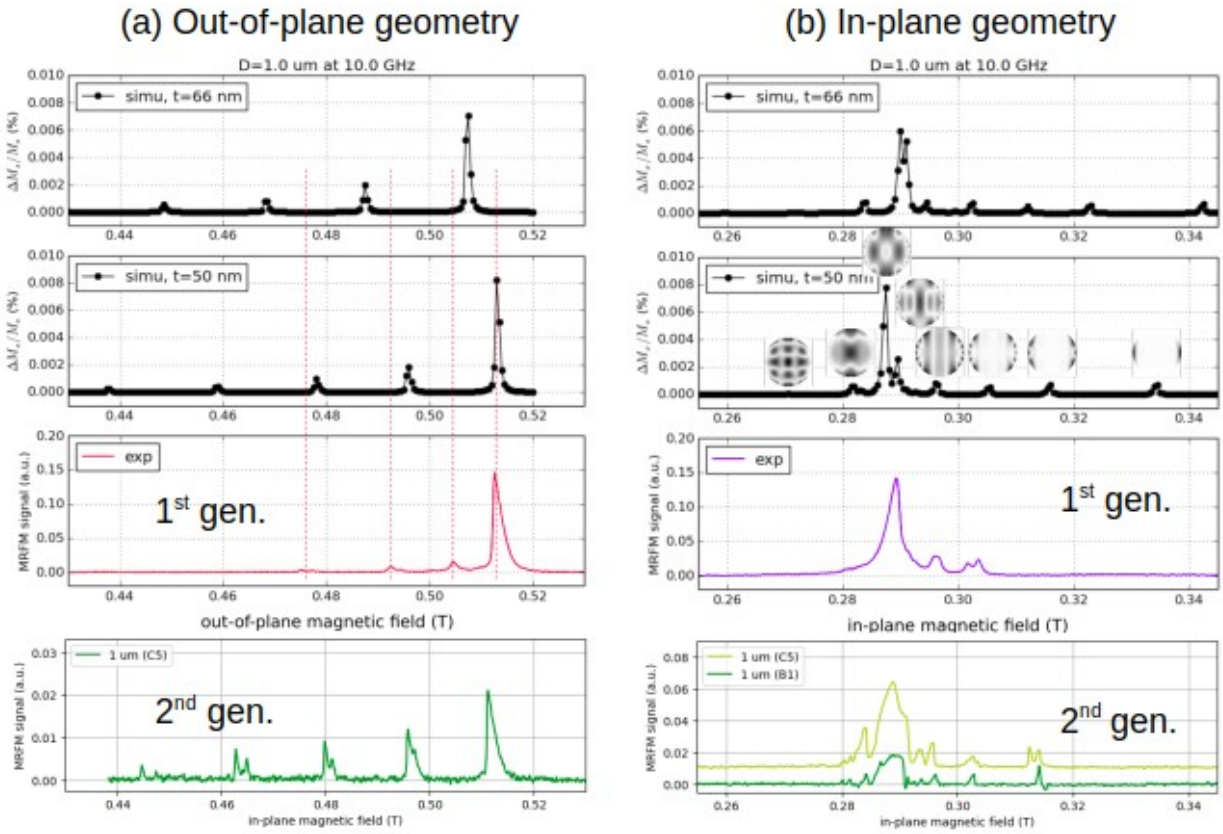

Figure 15. *Comparison between micromagnetic simulations (top two rows) and MRFM SW spectroscopy (bottom two rows) of the first and second generation YIG microsdisks of diameter 1 µm in the out-of-plane (a) and in-plane (b) configurations.*

3.1.3 Dependence of damping on diameter

Using broadband MRFM spectroscopy in the out-of-plane configuration, we extract the damping of the different microdisks, as a function of their diameter. The right panel of **Figure 16** displays a summary of this study, which was performed both on disks located underneath the rf antennas, and beside them.

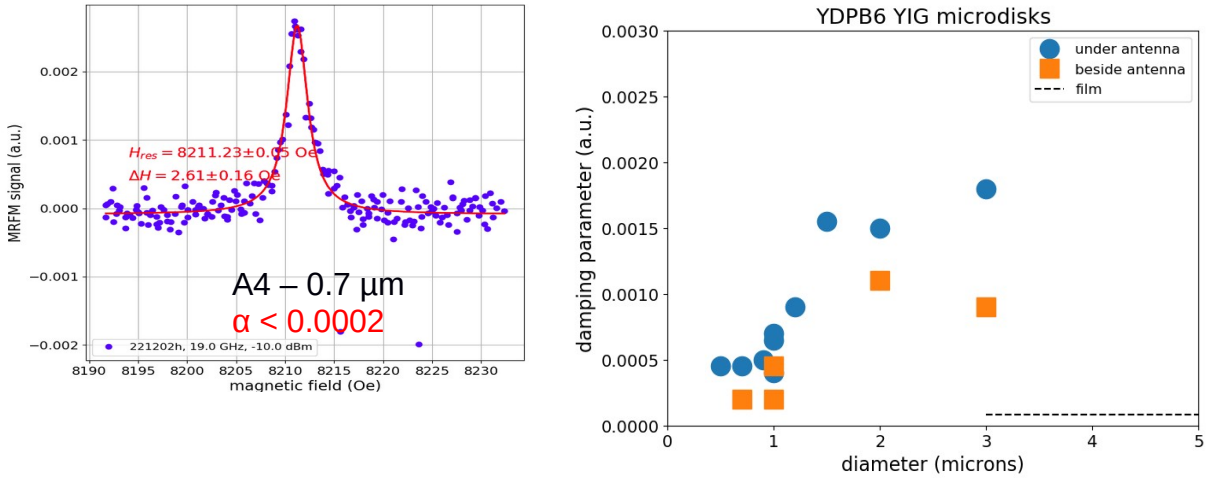

Figure 16. *Left: Main resonance line of the 0.7 µm diameter disk located next to the antenna, recorded at 19 GHz. Right: Evolution of the damping parameter extracted from broadband MRFM spectroscopy as a function of disk diameter. The dashed line shows the damping measured in the thin film.*

The evolution of damping on disk diameter in the second generation of samples is found to be in strong contrast with the one previously determined for the first generation (cf. **Figure 4**). It is found that the

damping of the disks located under the antennas increases from 5 10^{-4} up to 1.8 10^{-3} as the disk diameter increases from 0.5 µm to 3 µm. Moreover, the damping of the disks located next to the antennas is systematically found to be lower than the disks of same diameter located under the antennas, as shown by the comparison between orange squares and blue dots in the right panel of **Figure 16**. Strikingly, the disks of diameter below 1 µm exhibit extremely narrow linewidths at high frequency, as shown by the left panel for the 0.7 µm disk, whose linewidth is found to be 2.6 Oe at 19 GHz, which would correspond to a damping of less than 2 10^{-4}, *i.e.*, very close to the value measured on the extended thin film (8 10^{-5}). This clearly shows that the issues met during the nanofabrication process have largely been addressed. We tentatively ascribe the increased damping for larger disks to radiation damping, which is an effect of the strong inductive coupling between the excitation line and large volume and high microwave susceptibility samples.

3.2 MRFM parametric SW mode spectroscopy of the 1 micron disk

3.2.1 Reduced parametric threshold

Parametric SW mode spectroscopy has been performed on the second generation of sample. **Figure 17** shows the results of an experiment on the 1 µm disk similar to the one shown in **Figure 7c**, *i.e.*, by sweeping the in-plane parallel bias field at a fixed pumping frequency of 4 GHz. One can immediately see that in the same parameter range, more modes, with lower threshold power, can be parametrically excited in the new samples. In particular the threshold power is reduced by over an order of magnitude, which is ascribed both to the reduced damping of the 1 µm disk, and to the narrower width of the rf antenna.

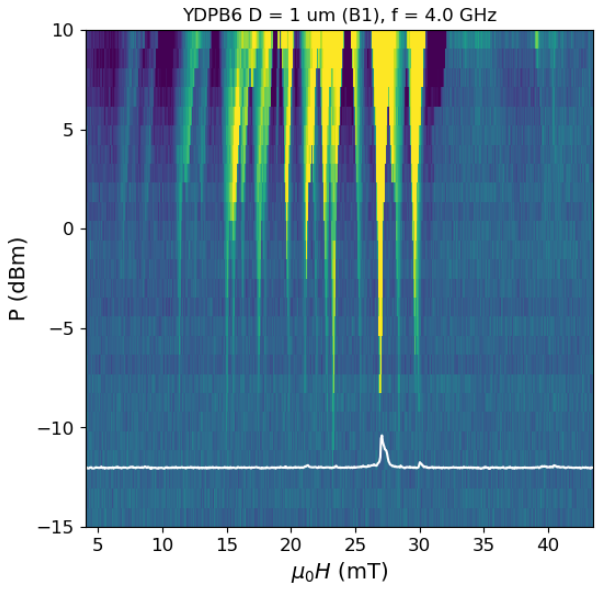

Figure 17. *Intensity map of the parametric modes in the field-power coordinates excited by the microwave field of frequency 4 GHz, measured by MRFM on the 1 µm diameter YIG disk. The continuous white curve corresponds to the direct excitation spectrum at the frequency of 2 GHz. The rf pumping field is at 45° from the dc field.*

3.2.2 Comparison to micromagnetic simulations

We compare the experimental parametric spectroscopy performed at a fixed in-plane bias field of 49 mT to the modes computed using the eigenmode solver in **Figure 18**. One observes a good overall agreement between the distribution of computed and experimental SW mode frequencies.

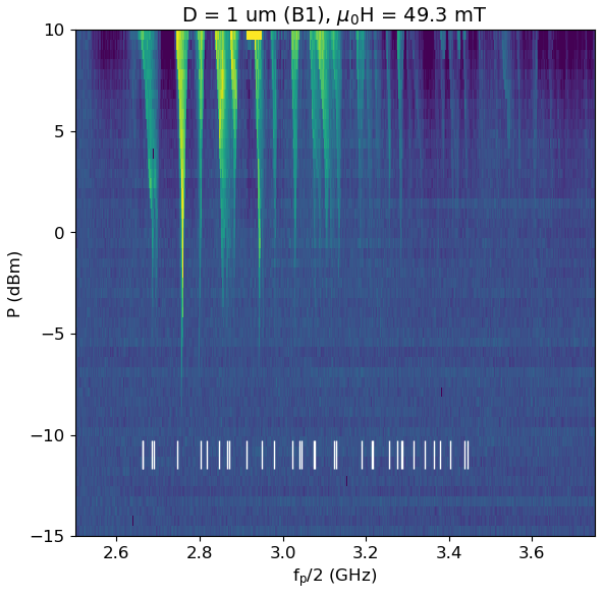

Figure 18. *Comparison between parametric spectroscopy MRFM data recorded at a fixed in-plane field of 49 mT (color-coded intensity map) and computed eigenfrequencies (white vertical ticks) for the 1 µm diameter disk.*

3.3 BLS magnon mode spectroscopy of the 500 nanometer disk

3.3.1 Expected mode structure

Figure 19 presents the computed eigenmodes for the YIG disk of diameter 500 nm magnetized by an in-plane field of 20 mT, using the normal magnon solver developed within k-NET. The simulation parameters are t = 52.2 nm, A = 3.57 pJ/m, M_s = 140 kA/m. The disk is discretized using cells of size 10 nm. It has also been checked, that the same mode structure is calculated using the mumax3 micromagnetic code.

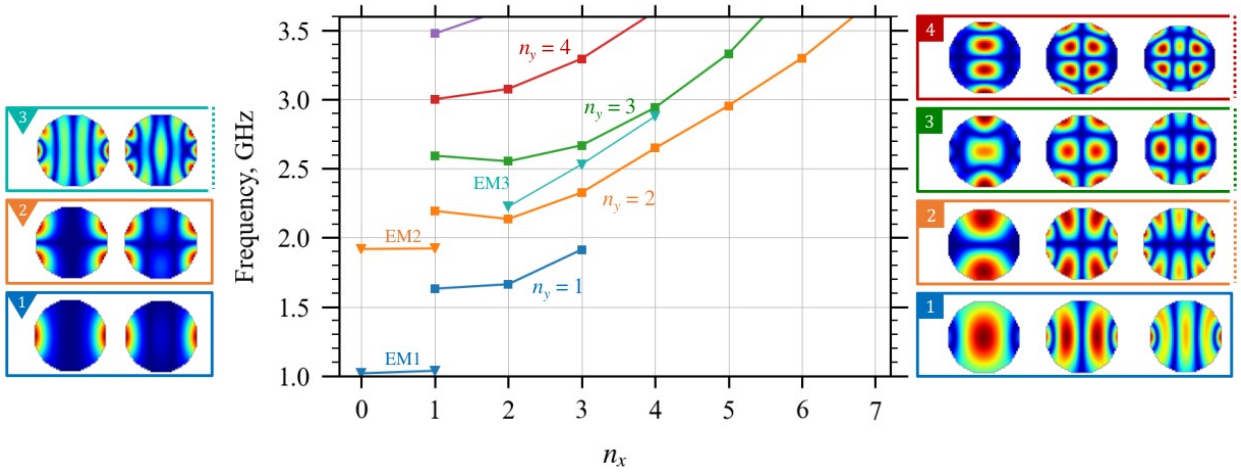

Figure 19. *Computed eigenmodes for the YIG disk of diameter 500 nm magnetized by an in-plane field of 20 mT applied along x. The central graph shows the frequency of the different edge mode (EM) and bulk mode (n_y) branches, as labeled. The spatial profiles of the edge modes (EM) are shown on the left, while those of the bulk modes are shown on the right.*

The notable characteristics of bulk modes are: i/ There are no modes (n_x, 1) with n_x > 3; ii/ Modes (n_x, 3) with n_x > 4 look close to what we would expect for those missing modes, likely due to hybridization; iii/ All branches tend to have stronger intensity at the edges as n_x increases.

The notable characteristic of edge modes (EM) are: i/ EM1 and EM2 are pairs of edge modes, one with zero contribution in the center, one with one lobe in the center of the disk; ii/EM3 is a hybrid edge mode, with n_y = 3 at the edges and n_y = 1 at the center. Its branch is limited by the n_y = 3 branch (with

other parameters, this branch can only have two modes); iii/ Edge modes with n_y > 3 are probably hybridized with the n_y = 2 bulk modes; iv/ The EM3 depends strongly on the thickness, but always has this "linear" alignment of the 3 modes. This can give us extra information for the identification of modes.

The 0.5 µm disk sample is too small to image the modes with BLS, therefore we have to identify the modes by their frequency and properties (relative intensities and nonlinear shift). For this purpose, we use linear direct excitation, thermal magnon spectrum and parallel pumping, as detailed below.

3.3.2 DIRECT LINEAR EXCITATION SPECTRUM

Firstly, we can directly excite some of the SW modes with the component of the rf field that is transverse to the static in-plane magnetization. **Figure 20** displays the BLS SW mode spectroscopy at very low power (P = 0.1 mW) to remain in the linear regime, the in-plane bias field being fixed to 20 mT. As expected, this SW mode spectrum is similar to those recorded by MRFM on same diameter disks at fixed frequency frequency while scanning the in-plane bias field, shown on the bottom row of **Figure 14**. As indicated by the vertical colored lines and insets, it is possible to identify straightforwardly 6 modes. We note that the experimental frequencies of the edge modes are shifted up by ~ 250 MHz compared to the computed ones.

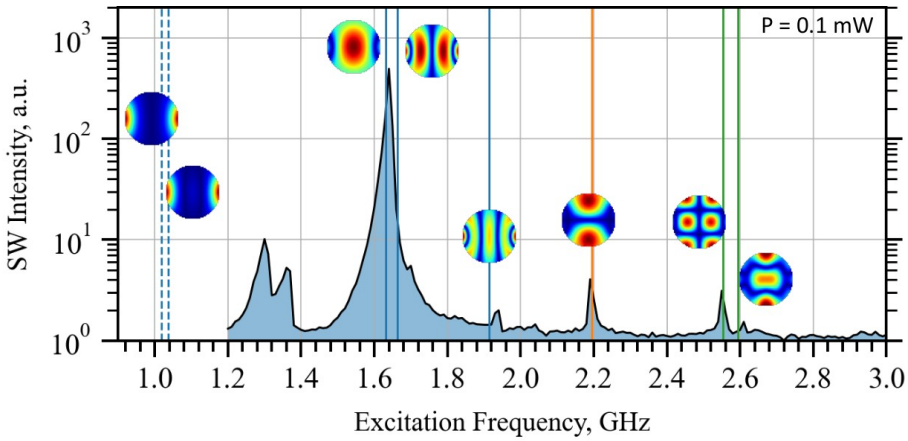

Figure 20. *BLS spectroscopy of the magnon modes directly excited by the transverse rf magnetic field produced by the antenna in the 500 nm YIG disk. The in-plane bias field is set to 20 mT.*

3.3.3 THERMAL MAGNON SPECTRUM

Thanks to the sensitivity of BLS spectroscopy, it is also possible to directly detect the SW modes that are thermally excited in the nanodisk, as shown in **Figure 21**. The advantage here is that all SW modes are populated independently of the symmetry of their spatial profile. The edge modes are identified with certainty when they are isolated from bulk modes (EM1, EM2, first and third EM3). The second edge mode of branch EM3 is deduced from the intensity of the thermal magnon spectrum and its near equidistant position from the two other EM3.

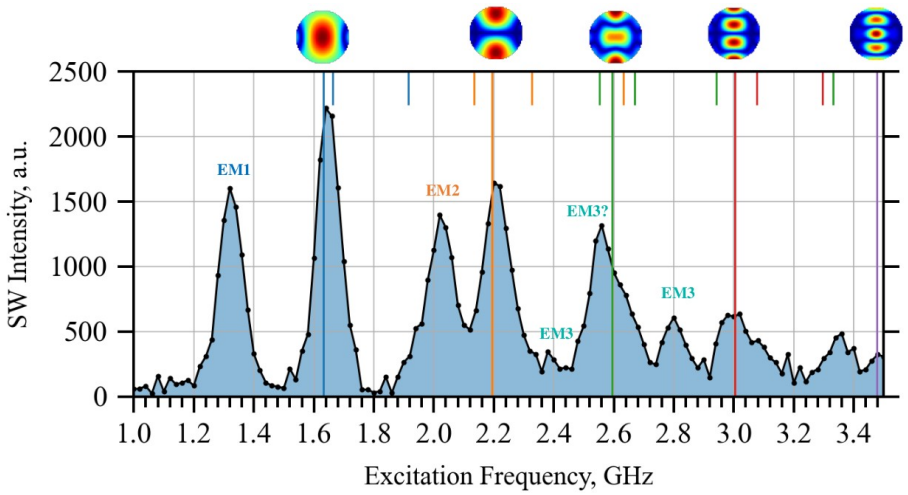

Figure 21. *BLS spectroscopy of thermal magnon modes in the 500 nm YIG disk for an in-plane bias field of 20 mT.*

3.3.4 PARALLEL PUMPING EXCITATION SPECTRUM

Finally, BLS spectroscopy was also used to detect the SW modes excited by parallel pumping. The obtained parametric mode spectra at two different powers, 1 mW and 10 mW, is shown in **Figure 22**. It is interesting to note that at higher power, we can distinguish the nonlinear shift. EM1 modes strongly shift up. Modes (1,1) and (2,1) shifts down strongly, while modes (3,1), (2,2), (1,2) and (3,2) only shift slightly down. Other edge modes are not sufficiently intense to demonstrate a shift.

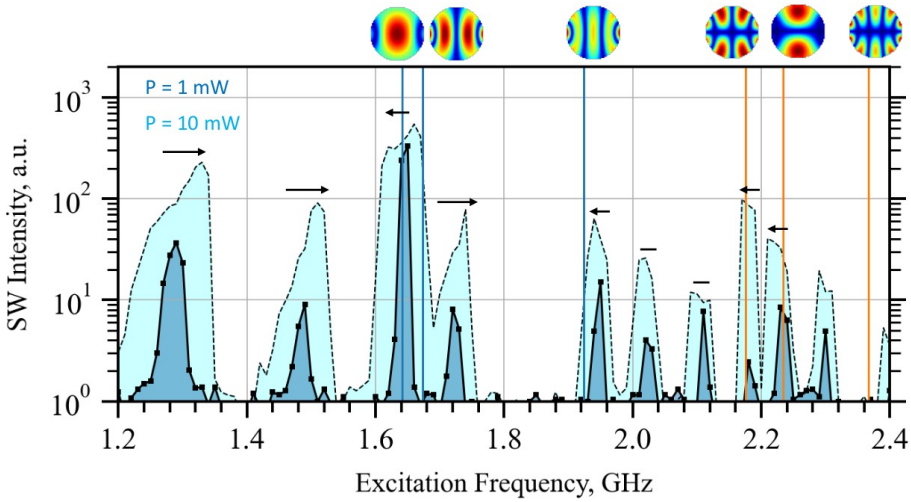

Figure 22. *BLS spectroscopy of the magnon modes parametrically excited by the component of the rf field parallel to the static magnetization of the 500 nm YIG disk. The in-plane bias field is set to 20 mT.*

3.4 Conclusion on the second generation of k-NET hardware

SW mode spectroscopy demonstrates an improved dynamical quality of the disks, and a much lower damping of smaller diameter disks. It yields a better understanding of SW mode spectrum of the smaller disks, both in linear and nonlinear regimes. The improved fabrication process that has been developed specifically for k-NET has proven to fulfill the requirements for strong nonlinear mode excitation at relatively low excitation powers (well below 1 mW), the actual power at the YIG disks being even lower if one considers insertions losses due to rf interconnections using wire bonding. Such powers are compatible with regular radiofrequency on-chip electronics that operate typically at a few mW.

4 GENERAL CONCLUSION AND OUTLOOK

Summary:

- Linear and parametric SW mode spectroscopy of k-NET devices vs. diameter performed by BLS and MRFM.
- 1st generation of k-NET devices: SW mode spectroscopy revealed a degradation of magnetic properties at the periphery of YIG disks due to nanopatterning (damping enhancement and absence of edge modes in experimental SW spectra). Still, a large number (> 10) of SW eigenmodes was identified on 3 µm diameter disks, thanks to the combination of experimental spectroscopy techniques and micromagnetic simulation codes (milestone M1.1).
- 2nd generation of k-NET devices: SW mode spectroscopy demonstrates an improvement of the of the previous shortcomings, thanks to an optimized nanofabrication process. Successful identification of SW eigenmodes (including edge modes) has been achieved on the smaller diameter disks (< 1 µm), whose damping remains close to its intrinsic value, resulting in much smaller nonlinear thresholds (< 1 mW). Still, enhanced damping is observed for larger disks, which is ascribed to radiation damping. The latter can be eliminated by minimizing the inductive coupling between the excitation antenna and the disk.
- Strongly nonlinear regimes of SW dynamics under transverse and parallel pumping can be achieved.

Outlook:

- The successful labeling of SW modes opens opportunities in using the normal mode approach in the nonlinear regime developed in WP3 (cf. Deliverable 3.1), *e.g.*, to understand experiments where several modes are simultaneously excited by distinct frequency signals, as well as the high power regime of parametric excitation, where distinct modes of frequencies close to $f_p/2$ can be excited by the microwave frequency f_p of the parallel pump. This will allow to extract the nonlinear coefficients between modes, which play the role of synaptic weights in the k-NN.
- Impact on the realization of the k-NET demonstrator: the present study addresses the simplest shape (= disks) and excitation schemes (= steady-state continuous excitations). Yet the obtained dynamics demonstrates the two principal requirements for implementing a practical k-NN computing device: complexity and discernability. Complexity relates to the number of accessible neurons and the depth of the nonlinear regime they can operate with moderate excitation power. The discernability allows to excite and read a chosen set of modes that are separated enough so to consider them formally as input neurons and output neurons.